STM JOURNALS

Journal of
Polymer & Composites

ISSN: 2321-2810 (Online)
ISSN: 2321-8525 (Print)
Volume 11, Special Issue 8, 2023
DOI (Journal): 10.37591/JoPC

http://engineeringjournals.stmjournals.in/index.php/JoPC/index

Research JoPC

Design and Analysis of A Metal Lined Composite Overwrapped Pressure Vessel

Kammili Harsha Naga Sai[1], Boggarapu Nageswara Rao[2], T. Parameshwaran Pillai[3], K.S. Sajikumar[4], K. Prasanth Kumar Reddy[5,*]

Abstract

This study presents a comprehensive investigation into the mechanical behavior of a metal lined composite overwrapped pressure vessel, designed for high-pressure storage applications. The design approach is dependent upon fiber material constants and dome shape factor. The study begins with obtaining dome coordinates and maintaining winding angles according to a geodesic path equation. Thickness estimation for the portion of cylindrical shell and domes are determined through netting analysis and cubic spline function respectively. The initial part of the study assesses hoop, axial, and effective stresses. Finite element modeling and analysis performed on several case studies to confirm the existing test data using ANSYS. The critically stressed cylindrical portion of the vessel governs the design. The netting analysis suggests a thickness of 4.59 mm for this section but considering 5 mm thickness (4 helical layers and 6 hoop layers). However, CLT analysis reveals that plies 1 to 4, with a 13.38° helical winding angle, fail due to exceeding the transverse filament strength, prompting the addition of supplementary plies to balance axial and hoop stresses. The resulting laminate design successfully meets all failure criteria, enhancing burst pressure and ensuring vessel reliability under a working pressure of 35 MPa with 1.5 safety factor.

Keywords: Cylindrical shell; Domes; Factor of Safety; Failure criterion; Fiber strength; Netting theory; Winding angle.

***Author for Correspondence**
K. Prasanth Kumar Reddy

[1]M. Tech Student, Department of Mechanical Engineering, Koneru Lakshmaiah Education Foundation (KLEF), Deemed to be University, Green Fields, Vaddeswaram, Guntur, Andhra Pradesh, India
[2]Professor, Department of Mechanical Engineering, Koneru Lakshmaiah Education Foundation (KLEF), Deemed to be University, Green Fields, Vaddeswaram, Guntur, Andhra Pradesh, India
[3]Assistant Professor, Department of Mechanical Engineering, University College of Engineering, BIT Campus, Tiruchirappalli, Tamil Nadu, India
[4]Associate Professor, Department of Mechanical Engineering, College of Engineering Trivandrum, Thiruvananthapuram, Kerala, India
[5]Research Scholar, Department of Mechanical Engineering, Koneru Lakshmaiah Education Foundation (KLEF), Deemed to be University, Green Fields, Vaddeswaram, Guntur, Andhra Pradesh, India

Received Date: November 28, 2023
Accepted Date: December 30, 2023
Published Date: February 01, 2024

Citation: Kammili Harsha Naga Sai, Boggarapu Nageswara Rao, T. Parameshwaran Pillai, K.S. Sajikumar, K. Prasanth Kumar Reddy. Design and Analysis of a Metal Lined Composite Overwrapped Pressure Vessel. Journal of Polymer & Composites. 2023; 11(Special Issue 8): S215-S232.

INTRODUCTION

As societies evolve and seek sustainable solutions, storing energy for use efficiently becomes paramount. Currently, a significant portion of the world's energy demand is met by fossil fuels, which not only have limited availability, but also contribute to environmental degradation, including CO_2 emissions, greenhouse gases, and subsequent global warming. In response, global initiatives, such as those undertaken by the European Union and unanimously decided at the G-7 summit in 2015, have set ambitious targets to completely eliminate fossil fuel consumption by the end of this century. At the same time, the aerospace industry continues to push the boundaries of innovation. Composite overwrapped pressure vessels (COPVs) exemplify this advancement, serving as critical components in aerospace applications, including spacecraft and communications satellites. These vessels are engineered to withstand the demands of containing high-pressure fluids in space, with weight being a

critical factor. COPVs offer a distinct advantage with their exceptional specific strength. Hydrogen will play a major role in various sectors, especially transportation, where about 90% of hydrogen energy is expected to be used. To fully establish hydrogen as a viable alternative to fossil fuels, the development of compact and safe storage methods is crucial, ensuring its safe and efficient use in various domains.

A COPV liner is usually made of a single vessel body that is cylindrical in shape with two end caps designed in an Isotensoid dome shape at either end of the cylinder. The term "Isotensoid" indicates that the tension within the fibers wrapped around the liner is the same in all directions. To accomplish this objective, aluminum liners can be fabricated using a combination of deep drawing and spinning processes, thereby producing both the liner and end caps from a single piece of material resulting in a reduction in the number of joints and the likelihood of leaks. Both the end caps and the body are wrapped with high-strength composite fibers by a filament winding technique where the fibers are embedded in a matrix which in this study is an epoxy resin. The metallic liner is supposed to act as a barrier to fluid ingress and does not necessarily exhibit any load bearing capabilities. The fibers are the primary load-carriers, and the matrix holds the fibers in place and transferring stress between them. It also protects the fibers from damage caused by environmental factors such as humidity or temperature.

LITERATURE SURVEY

The optimum geometry of the filament-wound pressure vessel is determined using continuum theory, composite properties and dome shape factor [1]. Madhavi and Rao [2] have used Clairaut's equation to calculate the optimum winding angle of fibers on a mandrel. By following a geodesic path, the fibers are able to distribute the load evenly over the entire surface of the vessel without slipping.

Alam et al. [3]investigated the effect of winding angle and stacking sequence on the burst strength of COPV using different failure criteria (such as maximum stress, maximum strain, Tsai-Hill, Tsai-Wu, and Hashin progressive failure). The Hashin damage criterion gives a reasonably accurate estimate of burst pressure. Optimal pole angle reported to be within 13° to 19°, and a hoop angle of 88.5°is recommended to achieve maximum pressure capability. An investigation by Kang et al. [4] revealed the importance winding angle of outer layers on the circumferential stress distribution in the cylindrical to dometransition region. They demonstrated the vulnerability of cylindrical region to failure under pressure by correlating test data with finite element analysis (FEA) results. They highlighted the critical role of wound patterns, particularly hoop wound fiber orientation, in determining burst strength and overall load-bearing capacity. Alam et al. [3] and Kang et al. [4] suggested winding of polar layers followed by winding of hoop layers.

Hu et al. [5] investigated both hoop and helical winding of the fibers on the cylindrical part of four-layer carbon fiber reinforced polymer composite pressure vessels. They predicted the burst pressure at different angles of fiber orientation and showed the best at an orientation angle of ± 45°. Iqbaletal. [6] analyzed the stress distribution and predictedthe burst pressure of filament wound composite pressure vessels with 30° to 60° fiber orientations using ANSYS. They showed high pressure capability at 40° fiber orientation angle. Yousaf et al. [7] reported an upward trend of up to 55°in the load-bearing capacity of the plies.

Netting analysis is used to estimate the thickness of the cylindrical section, while the thickness of dome section varies with the dome radius and winding pattern. A simple relationship that existed for the thickness of the dome resulted in an unrealistically infinite thickness at the pole. To solve this issue, a graphical technique suitable for small-sized pressure vessels was developed. Analytical equations of Knoell [8] underestimated the thickness. Wang [9] modified the equations and tested their adequacy with measured thicknesses. These equations were not suitable for the regions adjacent to the dome apertures, where filament buildup is more pronounced. For accurate finite element

modeling of composite pressure vessels, the cubic spline function appears to be valid only within two band widths of the pole to dome. Vasiliev et al. [10] proposed a relationship for the thickness of the dome that extends twice the width of the supporting band and continues to the cylindrical section.

Pavan and Ahmed [11] performed the finite element analysis and obtained high burst strength of COPV with minimum liner thickness and maximum composite thickness. High stiffness of COPV can be achieved with equal thickness of liner and composite shell. Zhang et al. [12] designeda hydrogen storage vessel to predict the burst pressure using the netting theory and employed a cubic spline function to minimize the accumulation of the dome thickness with polar radius. Radhika et al. [13] performed an internal hydrostatic pressure test by mounting strain gauges to measure circumferential and longitudinal strainson a carbon fiber reinforced polymer composite pressure vessel (having composite layer thickness of 1 mm). Vessel rupture between 106 and 108 bars indicates progressive ply-by-ply failure. The dome junction failed in hoop direction recording a failure strain of 16500 microns. This indicates the prevention of catastrophic failure in composite vessels.

Shivamurthy et al. [14] fabricated 10 COPVs for natural gas storageand tested them under a cyclic pressure of 3.5 MPa for 13,000 cycles (at 10 cycles/minute) and found no leaks. The vessels were pressurized to 1.25 times the service pressure for 5000 cycles at the same rate and no leakage was found until rupture. This shows the maximum pressure the vessels can withstand before rupturing. During pressure testing, matrix cracking results in gas leakage and prevents catastrophic failure of the COPVs. Ashok et al. [15] adopted the Tsai-Wu failure criterion and analyzedthe burst pressure of CFRP pressure vessels with varying fiber orientation angle. The optimal fiber orientation angle was determined to be within ±25°. Kangal et al. [16] designed COPV for high-pressure gas storage. They noted that hybridization has a negligible effect on burst pressure. The 3D finite element model predicts the burst pressure near to the recorded test data. Yeh and Liu [17] performed FEA and obtained the stress distributions inside symmetrical cross-ply graphite/epoxy composite pressure vessels under an internal pressure of 20 MPa. They evaluated the failure mode by applying the Tsai-Hill criterion and the maximum stress criterion.

Pramod et al. [18] designed an optimal spherical liner and discussed the composite overwrap requirement using FEA. They found that debond locations in the COPV increased liner failure. Minimized debonds by introducing 1 mm elastomer. The liner is protected from severe deformation and buckling. The manufacturing and joining techniques used in the assembly of COPV were satisfactory, and the weld areas were protected from failure. Nirbhay et al. [19] used the modeling techniques to investigate the failure of CNG cylinders. Carbon/epoxy provides a high safe working stress of 1498 MPa. Hoop winding was found to be superior in stress-carrying capacities for all-carbon and all-glass layers. Park and Kim [20] presented a method for creating composite layers in a high-pressure hydrogen vessel and applied classical laminated theory (CLT) to evaluate stress in individual layers.

Objective of the Present Study

The primary goal of this study focused on the design of COPVs specifically for high-pressure storage applications. This design approach rests on the continuum principle taking into account the fiber material constants and the dome shape factor. The initial phase involves the dome profile to maintain the winding angle in alignment with the geodesic path equation. The cylinder and the dome thicknesses were obtained using a combination of netting analysis and cubic spline functions. Hoop, axial, and effective stresses were estimated from dome profiles, radius of curvature, thickness and winding angle. A series of specific case studies performed to validate finite element models, failure criteria and results. By integrating the finite element analysis, and material models, this study establishes a basis for the design and evaluation of COPVs for high-pressure applications.

MATERIALS AND METHODS

The COPV is constructed using an aluminum alloy with bi-linearity, including a T700 carbon/epoxy composite material, wound around an aluminum liner. Mechanical properties of aluminum alloy liner and T700 carbon/epoxy are in Table 1 and Table 2 respectively.

Table 1. Mechanical properties of aluminum liner.

Properties	Value
Young's modulus	71 GPa
Poison's ratio	0.33
Yield Strength	276 MPa
Tangent Modulus	500 MPa

Table 2. Mechanical properties of T700/carbon epoxy [12].

Properties	Value
Extensional modulus in 2-direction (E_{22})	7420 MPa
Extensional modulus in 3-direction (E_{33})	7420 MPa
Shear Modulus (G_{12})	3710 MPa
Shear Modulus (G_{23})	3710 MPa
Shear Modulus (G_{13})	4790 MPa
Poisson's ratio (μ_{12})	0.28
Poisson's ratio (μ_{23})	0.28
Poisson's ratio (μ_{13})	0.3
Longitudinal tensile Strength (X_t)	2300 MPa
Longitudinal compressive Strength (X_c)	1250 MPa
Transverse Tensile Strength in (Y_t)	74 MPa
Transverse compressive (Y_c)	180 MPa
Developed fiber strength ($\boldsymbol{\sigma}_f$)	2800 MPa

Coordinates for the Dome Profile

It is assumed that no friction is present between the liner and the filaments. To avoid slippage of the fibers on the surface of revolution, the pre-stressed filaments follow the geodesic path given by Eq.1

$$y\,sin\alpha = Constant \tag{1}$$

Here, y is the radial distance and α is the winding angle made by the filament with the meridional line of the liner.

The Clairaut equation for thewinding angle is:

$$\alpha = \sin^{-1}\left(\frac{y_0}{y}\right) \tag{2}$$

Here, y_0 is the polar radius (or opening radius) of the pressure vessel. The winding angle, α is constant in the cylindrical region, while it varies with respect to the radial distance in the dome region. The geodesic path equation is not applicable as the filament reaches the vicinity of the pole while winding. At that region $\alpha = \frac{\pi}{2}$.

So, the geodesic path equation at the pole ($y_i = y$) becomes:

$$y\sin\alpha = y_i \tag{3}$$

Here, y_0 is pole opening radius; y_i is the minimum radius; and y_u is the maximum or cylindrical radius of the vessel (see Figure 1). The slight slope between the minimum radius and pole opening is intended to prevent the composite-overwrap layers from slipping off the ends of the vessel. The geometry of the dome is influenced by the orthotropic material constants of the composite and dome shape factor "q".

A vessel is typically a thin-walled structure that can be analyzed using the membrane theory. However, the vessel wall is composed of several layers wound at different winding angles, which vary

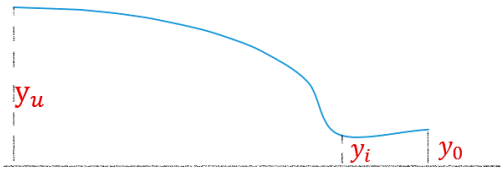

Figure 1. Geometric parameters of the vessel.

over wall thickness. Although the change in winding angle is assumed to be negligible, the wall consists of the same number of layers with equal thickness and elastic properties. As a result, the laminate is anti-symmetric with respect to its middle plane, leading to coupling between in-plane and out-of-plane forces and displacements. However, due to the symmetry of element at a given load, the constitutive equations for such an element can be simplified. The assumptions made for this analysis allow for a simple mathematical model but should be taken with caution as they may not fully represent the behavior of areal structure. This mathematical model considers a plane element ina bi-axial stresses which are given by

$$\begin{bmatrix}\sigma_1\\ \sigma_2\end{bmatrix} = \begin{bmatrix}C_{11} & C_{12}\\ C_{12} & C_{22}\end{bmatrix}\begin{bmatrix}\varepsilon_1\\ \varepsilon_2\end{bmatrix} \tag{4}$$

$$\sigma_1 = \frac{PR_2}{2t} = C_{11}\varepsilon_1 + C_{12}\varepsilon_2 \tag{5}$$

$$\sigma_2 = \frac{PR_2}{2t}\left(2-\frac{R_2}{R_1}\right) = C_{12}\varepsilon_1 + C_{22}\varepsilon_2 \tag{6}$$

Here, σ_1 and σ_2 are the axial and hoop stresses;ε_1 and ε_2 are the axial and circumferential strains; P is the working pressure; R_1 and R_2 are meridional and circumferential radius of curvatures:

$$R_1 = \frac{-\left\{1+\left(\frac{dy}{dx}\right)^2\right\}^{3/2}}{\frac{d^2y}{dx^2}} \tag{7}$$

$$R_2 = y\left\{1+\left(\frac{dy}{dx}\right)^2\right\}^{1/2} \tag{8}$$

The elastic stiffness constants (C_{11}, C_{12} $and C_{22}$) that describe the relationship between the principal stress and principal strain are:

$$C_{11} = \frac{(E_{11}\cos^4\alpha + E_{22}\sin^4\alpha + 2\mu_{21}E_{11}\sin^2\alpha\cos^2\alpha)}{1-\mu_{12}\mu_{21}} + G_{12}\sin^2 2\alpha \tag{9}$$

$$C_{12} = \frac{(E_{11}+E_{22})\sin^2\alpha\cos^2\alpha) + \mu_{21}E_{11}(\cos^4\alpha+\sin^4\alpha)}{1-\mu_{12}\mu_{21}} - G_{12}\sin^2 2\alpha \tag{10}$$

$$C_{22} = \frac{(E_{11}\sin^4\alpha + E_{22}\cos^4\alpha + 2\mu_{21}E_{11}\sin^2\alpha\cos^2\alpha)}{1-\mu_{12}\mu_{21}} + G_{12}\sin^2 2\alpha \tag{11}$$

Isotensoid shape is considered as the optimal design for the end closures and the stress levels along the fiber remain identical resulting uniform strains. Hence, the axial and circumferential strains (ε_1 and ε_2) are equal.

From the relationship between hoop and axial stresses,

$$\frac{\frac{PR_2}{2t}\left(2-\frac{R_2}{R_1}\right)}{\frac{PR_2}{2t}} = \frac{C_{12}\varepsilon_1 + C_{22}\varepsilon_2}{C_{11}\varepsilon_1 + C_{12}\varepsilon_2} \tag{12}$$

Using 7) and (8), and the condition, $\varepsilon_1 = \varepsilon_2$ in equation (12), one can write

$$\frac{C_{22}-2C_{11}-C_{12}}{C_{11}+C_{12}} = \frac{y\frac{d^2y}{dx^2}}{\left\{1+\left(\frac{dy}{dx}\right)^2\right\}} \tag{13}$$

Equation (13) provides the isotensoid dome shape. Using (9) to (11) in (13), one can write

$$\frac{E_{11}(\sin^2\alpha-2\cos^2\alpha)+E_{22}(\cos^2\alpha-2\sin^2\alpha)-\mu_{12}\mu_{21}}{E_{11}\cos^2\alpha+E_{22}\sin^2\alpha+\mu_{21}\mu_{12}}=\frac{y\frac{d^2y}{dx^2}}{\left\{1+\left(\frac{dy}{dx}\right)^2\right\}} \tag{14}$$

Introducing the dimensionless parameters: $X=\frac{x}{y_0}$; $Y=\frac{y}{y_0}$; $\sin\alpha=\frac{y_0}{y}=\frac{1}{Y}$;$\frac{dy}{dx}=\frac{dY}{dX}$;$\frac{d^2y}{dx^2}=\frac{d^2Y}{dX^2}$; $\sin^2\alpha=\frac{1}{Y^2}$;$\cos^2\alpha=1-\frac{1}{Y^2}$; the Maxwell's law of composites:$\frac{E_{22}}{E_{11}}=\frac{\mu_{21}}{\mu_{12}}$ in (14), one can write

$$\frac{1}{Y}\left[\frac{3(1-\frac{\mu_{21}}{\mu_{12}})+Y^2(\frac{\mu_{21}}{\mu_{12}}-2-\mu_{21})}{(\frac{\mu_{21}}{\mu_{12}}-1)+Y^2(1+\mu_{21})}\right]=\frac{\frac{d^2Y}{dX^2}}{\left\{1+\left(\frac{dY}{dX}\right)^2\right\}} \tag{15}$$

Defining a = $\left[\frac{\mu_{21}}{\mu_{12}}-\mu_{21}-2\right]$, b = $\left[1-\frac{\mu_{21}}{\mu_{12}}\right]$, c = $[1+\mu_{21}]$, d = $\left[\frac{\mu_{21}}{\mu_{12}}-1\right]$, the left hand side of equation (15) is simplified using partial fractions in the form

$$\Rightarrow\frac{ay^2+b}{y(cy^2+d)}=\frac{ay^2+b}{y(y^2+\frac{d}{c})}=\frac{A}{y}+\frac{By+C}{(y^2+\frac{d}{c})}\Rightarrow\frac{a}{c}y^2+\frac{b}{c}=A(y^2+\frac{d}{c})+\mathrm{B}y^2+Cy$$

Comparing terms on both sides:$\frac{a}{c}=A+B;\ Cy=0\Rightarrow$ C = 0; A = $\frac{b}{d}$; B = $\left(\frac{a}{c}-\frac{b}{d}\right)$

Equation (15) can be re-written in the form

$$\frac{-3}{Y}+\left[\frac{\mathrm{C}_2Y}{Y^2-\mathrm{C}_1}\right]=\frac{\frac{d^2Y}{dX^2}}{\left\{1+\left(\frac{dY}{dX}\right)^2\right\}} \tag{16}$$

Here, $\mathrm{C}_1=\frac{\left(1-\frac{\mu_{21}}{\mu_{12}}\right)}{(1+\mu_{12})}$ and$\mathrm{C}_2=\frac{\left(\frac{\mu_{21}}{\mu_{12}}-2-\mu_{21}\right)}{(1+\mu_{12})}+3$.

Multiplying (16) by $2\frac{dY}{dX}$, one can get after integration

$$\frac{dY}{dX}=\pm\frac{\{C(Y^2-\mathrm{C}_1)^{\mathrm{C}_2}-Y^6\}^{\frac{1}{2}}}{Y^3} \tag{17}$$

Since $\frac{dY}{dX}$ is a real quantity. The square root in (17) must be greater than zero.

$$\Rightarrow C(Y^2-\mathrm{C}_1)^{\mathrm{C}_2}\geq Y^6\Rightarrow \mathrm{f}(Y^2)=C(Y^2-\mathrm{C}_1)^{\mathrm{C}_2}-Y^6 \tag{18}$$

Real roots of f (Y^2) = 0 are in between $Y_i{}^2 and\ Y_u{}^2$. Assuming

$$Y^2=Y_i{}^2\sin^2\theta+Y_u{}^2\cos^2\theta \tag{19}$$

Differentiating (19) on both sides

$$\Rightarrow(2Y)dY=Y_i{}^2(2\sin\theta\cos\theta)d\theta\text{-}Y_u{}^2(2\sin\theta\cos\theta)d\theta$$

$$\Rightarrow \mathrm{YdY}=\left(Y_i{}^2-Y_u{}^2\right)(\sin\theta\cos\theta)d\theta$$

$$\Rightarrow\frac{dY}{dX}=-\frac{\{(Y_u{}^2-Y^2)(Y^2-Y_i{}^2)(Y^2+Y_i{}^2+Y_u{}^2)\}^{\frac{1}{2}}}{Y^3} \tag{20}$$

$$\Rightarrow X=-\int_{Y_u}^{Y}\frac{Y^2(YdY)}{\{(Y_u{}^2-Y^2)(Y^2-Y_i{}^2)(Y^2+Y_i{}^2+Y_u{}^2)\}^{\frac{1}{2}}}$$

$$= -\int_0^{\theta} \frac{(Y_i{}^2 \sin^2\theta + Y_u{}^2 \cos^2\theta)(Y_i{}^2 - Y_u{}^2)(\sin\theta\cos\theta)d\theta}{\{(Y_u{}^2 - Y_i{}^2\sin^2\theta - Y_u{}^2\cos^2\theta)(Y_i{}^2\sin^2\theta + Y_u{}^2\cos^2\theta - Y_i{}^2)((Y_i{}^2\sin^2\theta + Y_u{}^2\cos^2\theta + Y_i{}^2 + Y_u{}^2)\}^{\frac{1}{2}}}$$

$$X = \int_0^{\theta} \frac{(Y_i{}^2 sin^2\theta + Y_u{}^2 cos^2\theta)d\theta}{\{Y_i{}^2(1+sin^2\theta) + Y_u{}^2(1+cos^2\theta)\}^{\frac{1}{2}}} \tag{21}$$

Implementing the dome shape factor, q = $\frac{Y_u{}^2}{Y_i{}^2}$ in (21) and simplifying

$$X = Y_i \int_0^{\theta} \frac{(q\,cos^2\theta + sin^2\theta)d\theta}{\{(1+sin^2\theta) + q(1+cos^2\theta)\}^{\frac{1}{2}}}$$

$$X = Y_i(2q+1)^{\frac{1}{2}}\left\{\int_0^{\theta}\left((1-\frac{q-1}{2q+1}sin^2\theta\right)^{\frac{1}{2}}d\theta - \frac{q+1}{2q+1}\int_0^{\theta}\left((1-\frac{q-1}{2q+1}sin^2\theta\right)^{\frac{-1}{2}}d\theta\right\}$$

$$\Rightarrow \mathrm{X} = Y_i(2q+1)^{\frac{1}{2}}\left\{E(2) - \frac{q+1}{2q+1}E(1)\right\} \tag{22}$$

Here $E(1)\ and\ E(2)$ are elliptic integrals of first and second kind. Assuming,

$E_{11} = 134000MPa; E_{22} = 7420MPa$;$\mu_{12} = 0.28$; $\mu_{21} = \frac{E_{22}}{E_{11}}$=0.015504;

$y_0 = 25.5$; the dome shape factor, q = 25; $\mathrm{C}_1 = \frac{\left(1-\frac{\mu_{21}}{\mu_{12}}\right)}{(1+\mu_{12})}$ =0.73799;

$\mathrm{C}_2 = \frac{\left(\frac{\mu_{21}}{\mu_{12}}-2-\mu_{21}\right)}{(1+\mu_{12})} + 3 = 1.26201$; and $\mathrm{C} = \frac{\mathrm{C}_1{}^{\mathrm{C}_1+1}\left(q^{\frac{3}{\mathrm{C}_2}}-1\right)^3}{\left\{(q-1)^{\mathrm{C}_2}\left(q^{\frac{3}{2}}-q\right)^{\mathrm{C}_1+1}\right\}}$=170.2368

The dimensionless parameters corresponding to maximum cylindrical radius and minimum radius of the vessel are given by

$$\mathrm{Y_i}^2 = \frac{\mathrm{C}_1\left(\mathrm{q}^{\frac{3}{\mathrm{C}_2}}-1\right)}{\left(\mathrm{q}^{\frac{3}{\mathrm{C}_2}}-\mathrm{q}\right)} \tag{23}$$

$$\mathrm{Y_u}^2 = \frac{\mathrm{qC}_1\left(\mathrm{q}^{\frac{3}{\mathrm{C}_2}}-1\right)}{\left(\mathrm{q}^{\frac{3}{\mathrm{C}_2}}-\mathrm{q}\right)} \tag{24}$$

From (23) and (24),Y_i =0.864214; Y_u =4.321072. Y_i and Y_u are characteristic radii, which are multiplied with y_0 to obtain the maximum cylindrical radius and minimum radius of the pressure vessel:y_u =110.1873; and y_i=22.60265. The radial points in between y_i and y_u are obtained from (19) and (22) in which each radial point corresponds to an elliptic angle, θ ranging from 0^0 to 90^0. Forθ =0^0,$Y = Y_u$ =4.321072 and X = 0. For $\theta = 10^0$, Y =4.25807 and X = 0.452978. Similarly, the characteristic radii X and Y for θ ranging from 0^0 to 90° are given in Table 3. Multiplying the results with$y_0 = 25.5$, the coordinates (x, y) obtained in Table 3 for the dome profile shown in Figure 2. Figure 3 shows the aluminum liner. The winding angle (**α**) refers to the angle at which the composite fibers are wound around the liner of the pressure vessel, relative to the longitudinal axis of the vessel, which are generated using (2) and presented in Table 3. The geodesic path equation is obtained by Clairaut's equation, and the slippage of the fibers can be avoided as long as $ysin\alpha$is constant. However, this condition is not valid at the vicinity of the pole where α = $\frac{\pi}{2}$. So, the geodesic path equation becomes ysinα = y_i at the vicinity of pole.

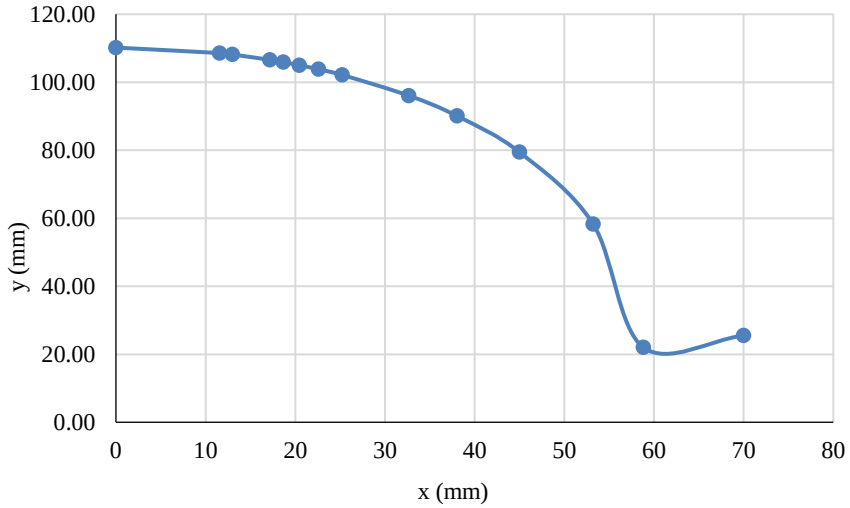

Figure 2. Plot of Isotensoid profile of dome.

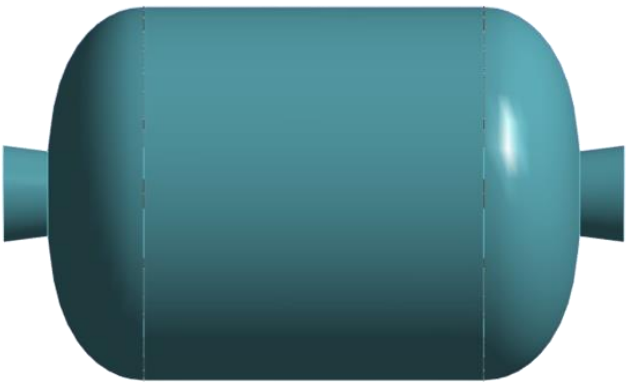

Figure 3. Aluminum liner.

Table 3. Generation of the data for the dome profile.

Elliptic angle, $\theta°$	E (1)	E (2)	X	Y	x (mm)	y (mm)	$\alpha°$
0	0	0	0	4.321	0	110.19	13.381
10	0.175	0.174	0.453	4.258	11.55	108.58	13.583
11.25	0.197	0.196	0.509	4.241	12.97	108.16	13.637
15	0.263	0.260	0.673	4.180	17.17	106.59	13.842
16.36	0.287	0.284	0.732	4.153	18.66	105.91	13.932
18	0.317	0.312	0.802	4.118	20.45	105.02	14.053
20	0.352	0.346	0.886	4.071	22.59	103.82	14.219
22.5	0.397	0.388	0.989	4.006	25.22	102.15	14.456
30	0.535	0.513	1.280	3.767	32.65	96.06	15.394
36	0.648	0.610	1.491	3.533	38.03	90.08	16.444
45	0.823	0.750	1.764	3.116	44.98	79.46	18.719
60	1.135	0.970	2.087	2.287	53.22	58.31	25.935
90	1.830	1.365	2.306	0.864	58.81	22.04	90

Dome Thickness of COPV

The dome section thickness a COPV variation depends on the specific design and manufacturing process. In general, the thickness increases gradually towards the inflection point of the dome (where the curvature of the dome changes from convex to concave). This high-stress region is due to a

change in curvature. Kumar et al. [21] reported that COPV with equal metal and composite layer yielded high bursting strength, whilePavan and Ahmed [11] remarked on thehighest stiffness of COPV. The highest burst strength of COPV can be achieved with minimum liner shell thickness and maximum composite shell thickness. Hu [22] considered an optimized netting theoryfor the thickness of the cylindrical section by taking account the stress balance coefficient. For the stress equilibrium factor, k = 1, the theory reduces to the traditional equilibrium conditional netting theory. So, k = 0.75 is considered. According to traditional netting theory, the thickness of the composite layer of the cylindrical section is

$$t_{\theta} = \frac{R_u P_{burst}}{2\sigma_f}(2 - \tan^2 \alpha) \tag{25}$$

$$t_{\alpha} = \frac{R_u P_{burst}}{2\sigma_f \cos^2 \alpha} \tag{26}$$

Here, $t_{\theta}$and t_{α} are thickness of hoop and helical layers;R_u=110.187 mmis the maximum radius of the liner; P= 70 MPa, is the burst pressure;and 35 MPais the working pressure. σ_f= 2800 MPa, is the fiber strength for whichwinding angle, α =13.38°. The thickness of the fiber is 0.5 mm and w = 2 mm is the fiber band width. Helical layers are used to compensate for the lower fiber strength in dome winding. this means that the thickness of the helical layers must be increased in the dome region. So, the optimized netting theory includes the stress balance coefficient (k) is [22]

$$t_{\theta} = \frac{R_u P_{burst}}{2\sigma_f}\left(2 - \frac{1}{k}\tan^2 \alpha\right) \tag{27}$$

$$t_{\alpha} = \frac{R_u P_{burst}}{2\sigma_f k \cos^2 \alpha} \tag{28}$$

Equations (27) and (28) used to determine the helical and hoop layer thicknesses (1.94 mm and 2.65 mm) to withstand the pressure of 70 MPa. The total thickness of the cylindrical composite shell was 4.59 mm with a roving thickness of 0.5 mm. For improved structural integrity and redundancy, the design was adjusted to include 4 helical layers and 6 hoop layers. The composite shell is designed to have a total thickness of 5 mm, with 4 helical plies and 6 hoop plies for added reinforcement while following the stacking sequence $[13.38°/-13.38°]_2$ and $[88.5/-88.5]_4$. In practical implementation, the cylinder incorporates a combination of both hoop winding and spiral winding, whereas the dome exclusively employs spiral winding due to geometric constraints. The methodology employed in thisproject consists of an initial winding of helical layers, followed by the sequential winding of hoop layers.

Moskvichev [23] presented a multi-zone lay-up simulation approach for composite winding, which is based on thickness calculation methods proposed by Vasiliev et al. [10] and Wang et al. [9]. The dome thickness from the inflection point to cylindrical section is [24]

$$t(r) = \frac{t_R R_u \sqrt{1-\frac{R_i}{R_u}}}{w}\left[\cos^{-1}\frac{R_i}{R} - \cos^{-1}\frac{R_i+w}{R}\right] \tag{29}$$

The dome thickness from minimum radius to the inflection point is [24]

$$t(r) = AR_i{}^0 + BR_i{}^1 + CR_i{}^2 + DR_i{}^3 \tag{30}$$

The dome thickness from equations (29) and (30) match well the measured thickness and can provide an accurate model for the FEA. Table 4 gives the thickness of the dome. Figure 4 shows a 2D axisymmetric model of COPV.

Analytical Solution

The axial (σ_1) and hoop or circumferential stress (σ_2) for the applied pressure (P) can be found from the radius of curvatures (R_1 and R_2) and the thickness of the shell using equations (5) and (6). From (16) and (17), R_1 and R_2 can be determined from the material properties and the derivatives of the

geometry ($\frac{dy}{dx}$and$\frac{d^2y}{dx^2}$), which are dependent on Y. Table 5 gives axial and circumferential stresses induced in the dome under internal pressure. Notably, the cylindrical section induces high hoop stresses, whereas the dome portion induces high axial stresses. Despite a continuous increase in circumferential radiusof curvature (R_2) from the cylindrical section to the pole, axial stress ($\boldsymbol{\sigma_1}$) only increases to a certain point and decreases thereafter due to thickness variation along the meridian. Hoop stress ($\boldsymbol{\sigma_2}$) exhibits minimal fluctuations. The derivation of analytic solutions for complex structural configurations involves considerable mathematical difficulties. The finite element method (FEM) has become one of the most popular and general numerical methods of structural analysis. Based on the nature of the final matrix equations, FEMs are often referred to as displacement method, force method and mixed method. The discrepancy between the results of FEA and the actual behavior of the structure, if any, may be due to improper selection of the elements, improper specification of boundary conditions and inadequate modeling of the structure.

Table 4. Dome thickness.

R (mm)	Thickness (mm)
110.187	5 (cylindrical section)
108.581	4.644
108.156	4.663
106.586	4.735
105.908	4.767
105.015	4.810
103.816	4.868
102.149	4.952
96.059	5.284
90.080	5.659
79.457	6.480
58.306	9.201
22.037	11.478 (vicinity of pole)

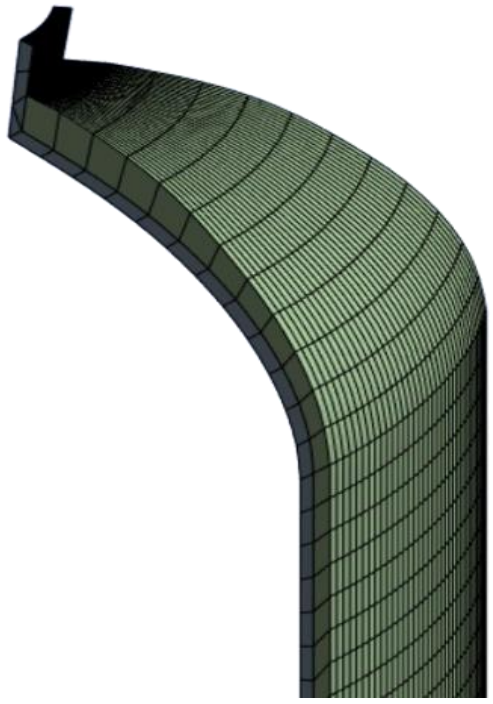

Figure 4. 2D axisymmetric model of COPV.

Case Studies

To assess the adequacy of FEM in ANSYS, case studies of metallic/composite rocket motor casings were employed in this section.

AFNOR 15CDV6 Steel Rocket Motor Case

A comparative study is made considering AFNOR 15CDV6 steel rocket motor case tested to burst under internal pressure as shown in Figure 5 [25–27].

FE model is generated for the highly stressed cylindrical shell portion of the rocket motor case (having inner radius = 103.3 mm and outer radius = 105.9 mm). Material properties specified are: Young's modulus = 202.7 GPa and the Poisson's ratio = 0.301. The hoop stress from the finite element analysis obtained for the internal pressure of 7.75 MPa is 305.3 MPa (see Figure 6), whereas it is 317.5 MPa from the experimental stress analysis. The discrepancy in the results may be due to changes in thickness and the diameter of the rocket motor casing under internal pressure.

Composite Motor Casing

An attempt is made to compare the hydro-proof pressure test results of a composite motor casing (see Figure 7) with FEA results.

Table 5. Axial (σ_1) and circumferential (σ_2) stresses in the dome.

Y	R_1	R_2	α°	σ_1 (MPa)	σ_2 (MPa)	σ_{eff} (MPa)
4.321	∞	110.19	13.381	385.66	771.31	667.98
4.258	66.05	111.26	13.583	419.24	132.29	371.21
4.241	66.24	111.56	13.637	418.64	132.29	370.65
4.180	66.98	112.68	13.842	416.41	132.28	368.53
4.153	67.30	113.17	13.932	415.44	132.28	367.60
4.118	67.73	113.82	14.053	414.14	132.29	366.37
4.071	68.32	114.71	14.219	412.38	132.30	364.70
4.006	69.15	115.98	14.456	409.89	132.33	362.32
3.767	72.44	120.88	15.394	400.32	132.60	353.21
3.533	76.05	126.15	16.444	390.12	133.16	343.48
3.116	83.72	136.82	18.719	369.47	135.16	323.79
2.286	107.26	164.17	25.935	312.25	146.58	270.59

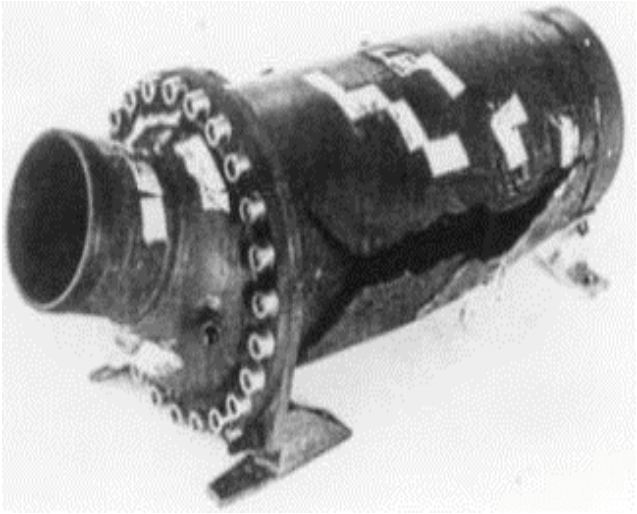

Figure 5. AFNOR 15CDV6 steel rocket motor casing after burst test.

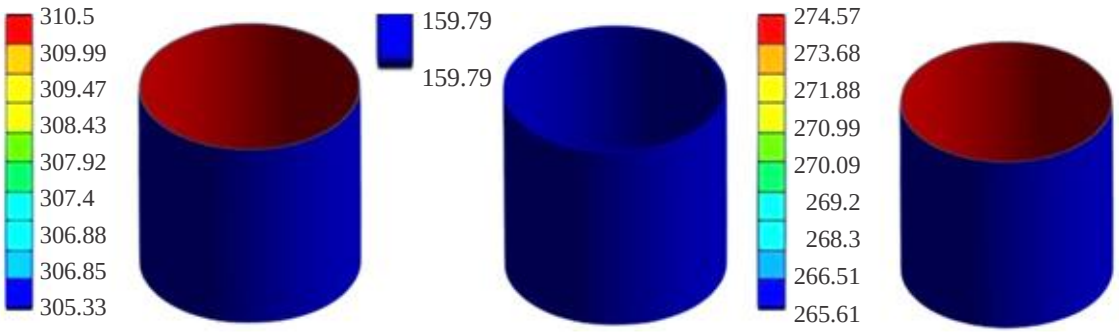

Figure 6. FEA stress contour plots of the AFNOR 15CDV6 steel rocket motor casing under internal pressure of 7.75 MPa.

Figure 7. Composite motor casing.

This multilayer structure is formed by winding several families of tapes in which every tape having a winding angle of $+\phi$, there is a corresponding tape at $-\phi$. One can treat this type of configuration as a balanced angle-ply laminate having no in-plane shear strains and extension-shear coupling. This type of multilayer structures can be modeled using shell element and specifying overall orthotropic properties to the layup sequence [27]:

$$E_{rr} = 4.336\ GPa;\ E_{\theta\theta} = 38.2904\ GPa;\ E_{zz} = 23.354\ GPa;\ G_{rz} = 1.027\ GPa;\ G_{r\theta} = 1.054\ GPa;\ G_{\theta z} = 2.958\ GPa;$$

$$\vartheta_{\theta z} = 0.2478;\ \vartheta_{rz} = 0.1014;\ \vartheta_{r\theta} = 0.0612$$

The inner radius of the casing is 980 mm and the average thickness of the cylindrical shell is 13mm. The measured hoop strain under proof pressure of 4.905 MPa in cylindrical portion of the composite motor casing is 12000 microns, whereas the FEA solution is 12228 microns (see Figure 8). The measured radial displacement is 11.5 mm, whereas the analysis result is 11.306 mm. FEA results are in good agreement with the measured values.

These two case studies confirm the adequacy of FE solutions in estimating the stresses and strains in rocket motor casings under different loading conditions.

Cylindrical Section of COPV

The analytical results of COPV in Section 2.3 are compared by FE modeling of the cylindrical section of COPV to ensure accuracy of FE solution. The inner diameter of the cylindrical section is 110.18 mm and thickness is 5 mm. The cylindrical vessel is subjected to the internal pressure of 35 MPa and a force of 1335000 N is applied on the upper edge to simulate the closed ends of the vessel.

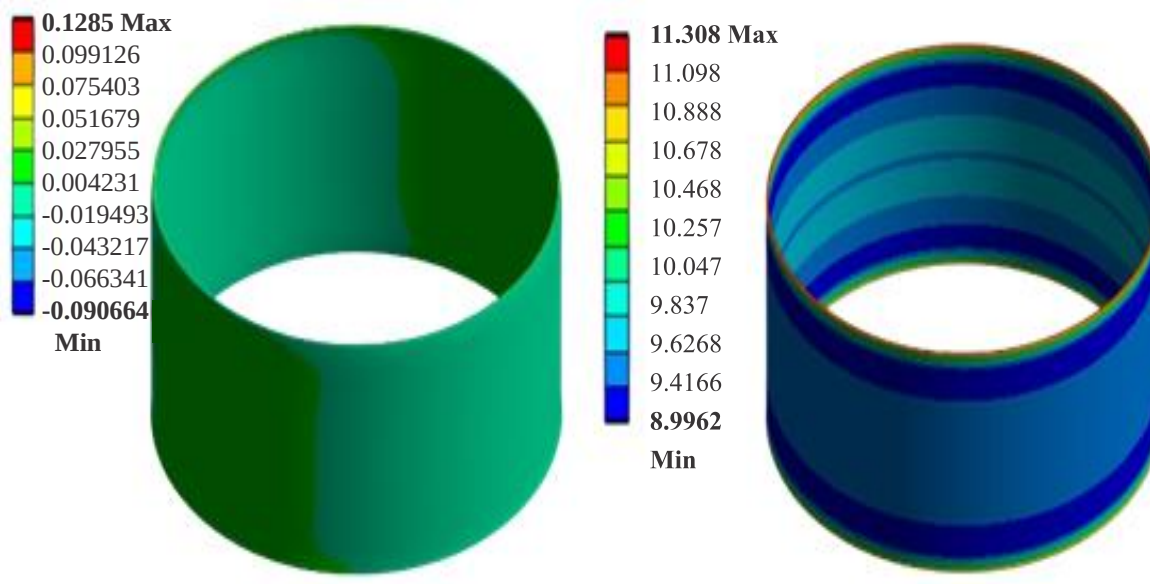

Hoop strain Total displacement

Figure 8. Stress and deformation contour plots of the composite motor casing under internal pressure of 4.905 MPa.

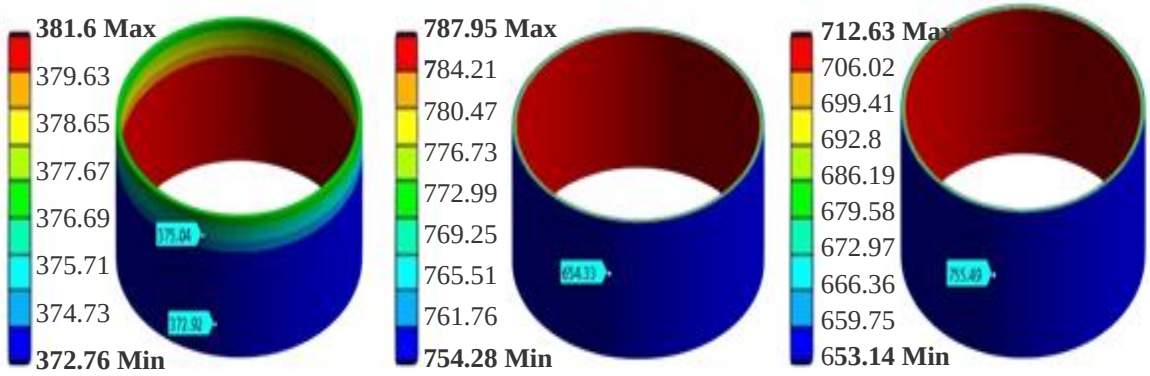

Axial stress Hoop stress Effective stress

Figure 9. Stress contour plots of the cylindrical shell portion of COPV.

The values of axial, hoop, and effective stress from the analytical solution in Table 5 for the cylindrical section of COPV are 385.65 MPa, 771.31 MPa and 667.97 MPa, respectively. Figure 9 shows the contour plots of the stress distribution. FEA solution matches well with the analytical solution.

Bursting Pressure of a Hydrogen Storage Vessel

Xu et al. [28] conducted the bursting pressure test on a hydrogen storage vessel. The cylindrical part is composed of a 6061-T6 aluminum liner with 10 layers of T700/carbon epoxy and createda 3D parametric finite element model to determine the failure pressure using the properties in [29] and the failure criteria [30]. Theyapplied the maximum stress criterion, Tsai-Hill criterion, Tsai-Wu criterion, and Hoffman criterion to predict the laminate's strength. The inner radius of the 1.8 mm thick liner is 44 mm. The thickness of each winding layer is 0.42 mm. The outer radius of the composite is 50 mm and the length of the cylindrical part is 160 mm. The winding angle of each composite layer from inner layer to outer layer is $\pm 90°$, $\pm 18.9°, \pm 90°, \pm 28.6°, \pm 90°$ respectively. The reported burst pressure of the vessel is within 125-126 MPa. Figure 10 shows the COPV after the burst test. Figure 11 shows the failure index contour of the vessel under the internal pressure of 120 MPa. Failure of

vessel initiates when the failure index exceeds 1. Maximum stress criterion and Tsai-Hill criterion indicate the failure index above 1, while the Tsai-Wu criterion indicates the failure index as 0.97103, which is close to 1. Table 6 gives the variation of failure index with applied pressure for different failure criteria.

The actual burst pressure of the vessel is between 125 MPa to 126 MPa. Numerical simulations with various failure criteria indicated the failure pressure close to 120 MPa, while the Tsai-Wu criterion indicated the failure index of 1 at 125 MPa, with the initial failure occurring within 90° ply orientation.

ANALYSIS OF METAL LINED COPV

CFRP composite is overwrapped (in 4 helical and 6 hoop plies of fiber thickness of 0.5 mm and a width of 2 mm constituting 9 mm cylindrical thickness) over a 4 mm thick aluminum alloy liner. Material non-linearity of the Al-liner (see Figure 12) is considered. The liner and the composite are bonded together. The liner transfers the load (internal pressure) to the overwrapped composite. Carbon fibers are the main load carriers. The internal pressure of 35 MPa is applied on the inner surface of the liner. Figure 13 shows how the liner is transmitting the load to the composite overwraps. The Al-liner shares the load up to the yield point and later on, transmits the load to the overwrapped composite. Stress in the liner increases with the strain up to yield point. Beyond yield, the strain in the liner increases with increasing internal pressure keeping the stress almost constant, which means the Al-liner undergoes deformation and straining without stress enhancement, and the load will be shared by the overwrapped composites.

Plies 1 to 4 (characterized by a helical winding angle of 13.38°) exceed the transverse strength of the filament and modified the design of cylindrical section with two additional plies (with a winding angle of 55°). None of the failure criteria exceeded the limit of the index with the modified design. Table 7 gives the variation of failure index with applied pressure for different failure criteria. Failure of the COPV initiates when the failure index exceeds 1. For the internal pressure of 55 MPa, Tsai-Hill, Tsai-Wu, Hoffman and Hashin criteria indicate the failure index above 1. The maximum-stress criterion indicates the failure index above 1 for the applied pressure of 60 MPa. From Table 7, the failure index values suggest that, under a working pressure of 35 MPa, the vessel is within the safety margin of 1.5. Figure 14 shows the Stress contour plots of the COPV under internal pressure of 35 MPa.

Figure 10. COPV after the burst test [28].

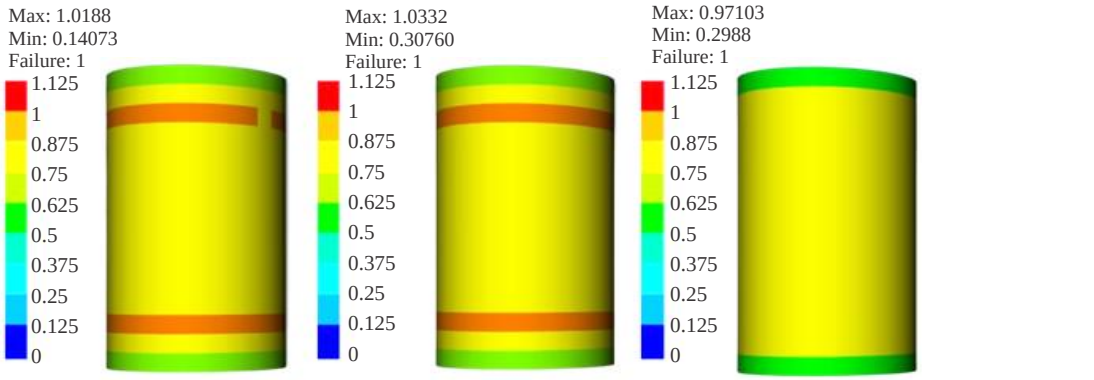

Figure 11. Failure index of the vessel at the internal pressure of 120 MPa.

Table 6. Variation of the failure index with applied internal pressure.

Pressure (MPa)	Maximum stress	Hoffman	Tsai-Hill	Tsai-Wu	Hashin
10	0.0661	0.0665	0.0665	0.0685	0.0661
20	0.1323	0.1331	0.1331	0.1371	0.1323
30	0.1986	0.1999	0.1999	0.206	0.1986
40	0.2654	0.2672	0.2672	0.2754	0.2654
50	0.3508	0.3531	0.3531	0.3639	0.3508
60	0.4409	0.4438	0.4438	0.4575	0.4409
70	0.5322	0.5357	0.5357	0.5539	0.5322
80	0.6241	0.6283	0.6283	0.6568	0.6241
90	0.7164	0.7212	0.7212	0.7615	0.7164
100	0.809	0.8143	0.8143	0.8665	0.809
110	0.9083	0.9439	0.9439	0.9	0.9083
120	1.0188	1.0332	1.0332	0.9955	1.0192
125	1.0675	1.0729	1.0729	1.0178	1.0675
130	1.1142	1.1183	1.1183	1.0716	1.1142
135	1.1612	1.1643	1.1643	1.1244	1.1612
140	1.208	1.2101	1.2101	1.1782	1.208
145	1.255	1.2563	1.2563	1.2232	1.255
150	1.302	1.3025	1.3025	1.2866	1.302
155	1.349	1.3489	1.3489	1.3408	1.3491
160	1.3964	1.3964	1.3964	1.3967	1.3964

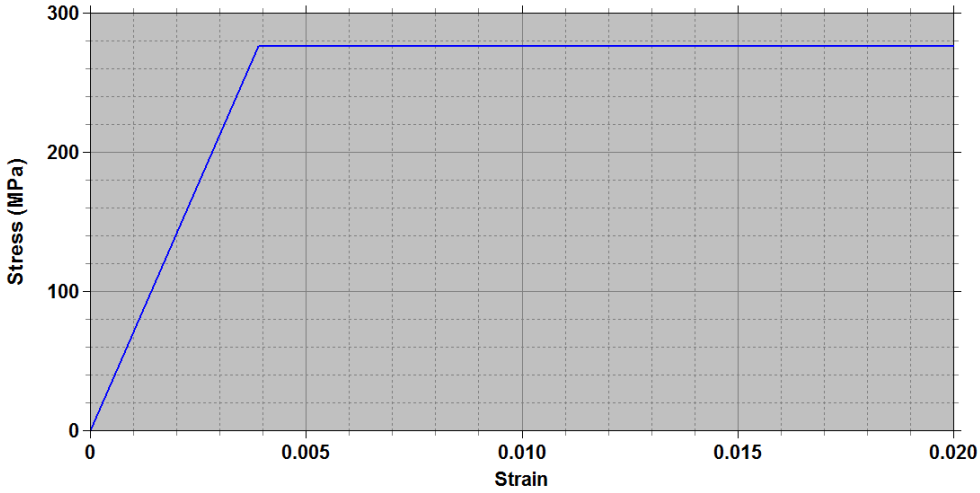

Figure 12. Stress-strain curve of the Al-liner.

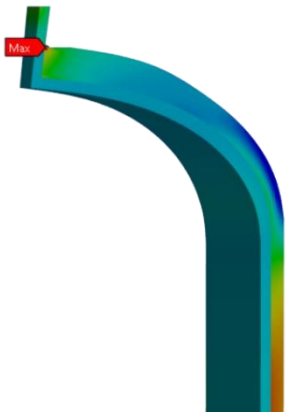

Figure 13. Load transmission capacity of the liner to the composite.

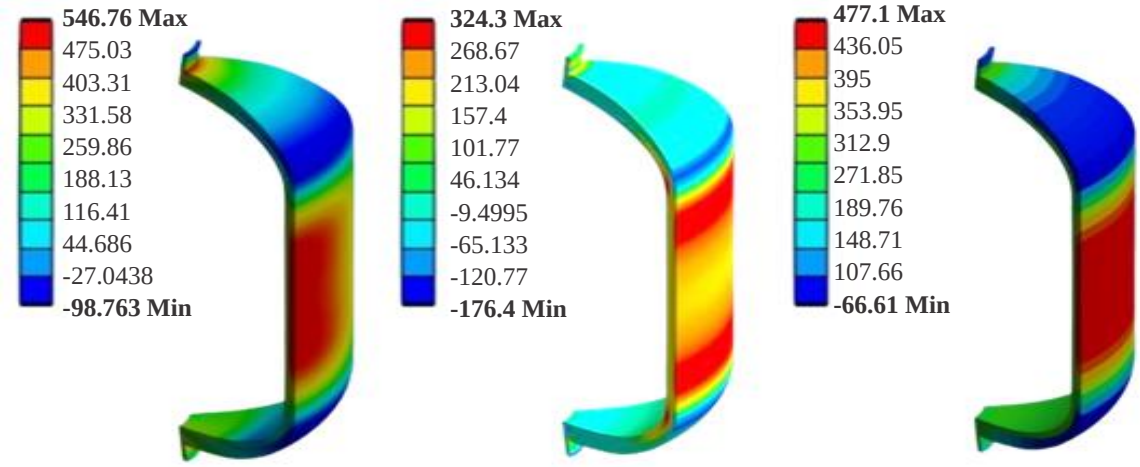

Hoop stress Axial stress Equivalent stress

Figure 14. Stress contour plots of the COPV under 35 MPa internal pressure.

Table 7. Variation of failure Index for COPV with applied pressure.

Internal pressure (MPa)	Failure index (FI) for each criterion				
	Maximum stress	***Tsai-Hill***	***Tsai-Wu***	***Hoffman***	***Hashin***
5	0.062	0.070	0.070	0.070	0.068
10	0.124	0.141	0.139	0.139	0.136
15	0.187	0.211	0.209	0.209	0.204
20	0.249	0.282	0.279	0.279	0.272
25	0.313	0.353	0.350	0.350	0.341
30	0.414	0.451	0.461	0.462	0.451
35	0.520	0.566	0.576	0.579	0.566
40	0.627	0.683	0.693	0.698	0.683
45	0.735	0.800	0.811	0.817	0.800
50	0.844	0.918	0.929	0.936	0.918
55	0.953	1.040	1.047	1.056	1.036
60	1.063	1.171	1.168	1.175	1.155
65	1.173	1.303	1.290	1.295	1.274
70	1.285	1.436	1.411	1.417	1.394
75	1.396	1.570	1.531	1.539	1.514
80	1.508	1.705	1.652	1.661	1.634

CONCLUSIONS

This paper deals with the mechanical behavior of a metal lined composite overwrapped pressure vessel (COPV) used for high-pressure storage applications. The consistent distribution of effective stress throughout the structure serves as confirmation of its classification as an Isotensoid dome. The coordinates of the dome profile are dependent on elliptic integrals of the first and second kind. Fiber slippage is avoided by implementing the geodesic path condition through Clauriot's equation. Netting analysis has been performed to determine the thickness of the cylindrical section. Empirical relations are used to estimate the thickness of the dome section. According to netting theory, employing 4 helical and 6 hoop plies is sufficient to withstand the working pressure of 35 MPa. Plies 1 to 4 (characterized by a helical winding angle of 13.38°) exceed the filament transverse strength. Design is modified (by using an extra two piles with a winding angle of 55°) and confirmed the failure index within the acceptable limit.

REFERENCES

1. Th.de Jong, "A theory of filament wound pressure vessels", Delft University of Technology, Department of Aerospace Engineering, Report LR-379 (1983).http://resolver.tudelft. nl/uuid:cb23830f-81c4-49d9-b6ee-cee2a429e6cb
2. M. Madhavi and K.V.J. Rao, "Computer aided analysis of filament wound composite pressure vessel with integrated end domes considering the change of winding angles through the thickness direction", Journal of the Institution of Engineers (India): Mechanical Engineering Division, Vol.91, pp.10-16 (2010).
3. S. Alam, G. R. Yandek, R. C. Lee, and J. M. Mabry, "Design and development of a filament wound composite overwrapped pressure vessel", Composites Part C: Open Access, 2 (2020) 100045 14 pages. https://doi.org/10.1016/j.jcomc.2020.100045
4. H. Kang, P. He, C. Zhang, Y. Dai, Lv. Hong, M. Zhang, D. Yang, "Stress–strain and burst failure analysis of fiber wound composite material high-pressure vessel", Polymers and Polymer Composites, Vol. 29, No. 8, pp.1291–1303 (2021).doi:10.1177/0967391120965387
5. Hu, J. Chen, S. Sundararaman, K. Chandrasekhara, and W. Chernicoff, "Analysis of composite hydrogen storage cylinders subjected to localized flame impingements", Int J Hydrogen Energy, Vol. 33, No. 11, pp. 2738–2746 (2008). doi:10.1016/j.ijhydene.2008.03.012
6. M.A.M. Iqbal, Md.H. Ali, and Md. Fareed, "Design and stress analysis of FRP composite pressure vessel", International Journal for Modern Trends in Science and Technology (IJMTST), Vol.2, Issue 2, pp.152-159 (2016).
7. H. Yousaf, M. Hamza, M. Sattar (2023). Design and analysis of acomposite pressurevessel.https://doi.org/10.36227/techrxiv.22979420.v1
8. A.C.Knoell, "Structural design and stress analysis program for advanced composite filament-wound axisymmetric pressure vessels/COMTANK/", https://ntrs.nasa.gov/citations/19710016892
9. R. Wang, W. Jiao, W. Liu, and F. Yang, "A new method for predicting dome thickness of composite pressure vessels", Journal of Reinforced Plastics and Composites, Vol. 29, No. 22, pp. 3345–3352 (2010). doi: 10.1177/0731684410376330.
10. V.V. Vasiliev, A.A. Krikanov, and A.F. Razin, "New generation of filament-wound composite pressure vessels for commercial applications", Compos Struct, Vol. 62, No. 3–4, pp.449–459 (2003).doi: 10.1016/j.compstruct.2003.09.019.
11. A.E. Pavan and K.S. Ahmed, "Effect of constituent shell thickness on burst pressure of composite overwrapped pressure vessel", International Journal of Scientific & Engineering Research (IJSER), Vol.9, Issue 5, pp.112-118 (2018).
12. Q. Zhang, H. Xu, X. Jia, L. Zu, S. Cheng, and H. Wang, "Design of a 70 MPa type IV hydrogen storage vessel using accurate modeling techniques for dome thickness prediction", Compos Struct, vol. 236 (2020) 111915, doi: 10.1016/j.compstruct.2020.111915.
13. M. Radhika, K. Chandra Shekar, and G. V Rao, "Design, Fabrication and Testing of Composite Overwrapped Pressure Vessel for CNG Storage", International Journal of Engineering Research & Technology (IJERT), Vol. 3, Issue 12, pp. 136-138 (2014).
14. B. Shivamurthy, Siddaramaiah, and M. S. Prabhu swamy, "Design, fabrication, and testing of epoxy/glass-reinforced pressure vessel for high-pressure gas storage", Journal of Reinforced

Plastics and Composites, Vol. 29, No. 15, pp. 2379–2386 (2010).doi: 10.1177/ 0731684409351169.
15. R. Ashok, R. Ranjith Kumar, and T. Rao, “Design and Analysis of CFRPcomposite multilayer high-pressurevessels andburst pressure analysis forvarious fiber orientation angles”, International Journal of Advanced Trends in Computer Science and Engineering, Vol. 2, No.1, pp. 602–607 (2013).
16. S. Kangal, O. Kartav, M. Tanoğlu, E. Aktaş, and H.S. Artem, “Investigation of interlayer hybridization effect on burst pressure performance of composite overwrapped pressure vessels with load-sharing metallic liner”, J Compos Mater, Vol. 54, No. 7, pp. 961–980 (2020).doi: 10.1177/0021998319870588.
17. M.K. Yeh and T.H. Liu, “Finite element analysis of graphite/epoxy composite pressure vessel”, Journal of Materials Science and Chemical Engineering, Vol. 5, No. 7, pp.19–28 (2017).doi: 10.4236/msce.2017.57003.
18. R. Pramod, C. K. Krishnadasan, and N. Siva Shanmugam, “Design and finite element analysis of metal-elastomer lined composite over wrapped spherical pressure vessel”, Compos Struct, vol. 224 (2019)111028. doi: 10.1016/j.compstruct.2019.111028.
19. M. Nirbhay, S. Juneja, A. Dixit, R.K. Misra, S. Sharma,“Finite element analysis of all composite CNG cylinders”, Procedia Materials Science, Vol.10, pp.507-512 (2015).https://doi.org/10.1016/j.mspro.2015.06.093
20. G. Park and C. Kim, “Composite layer design using classical laminate theory for high pressure hydrogen vessel (Type 4)”, International Journal of Precision Engineering and Manufacturing, Vol. 24, No. 4, pp. 571–583 (2023).doi: 10.1007/s12541-022-00752-w.
21. G.C. Kumar, M. Sagar, A.C.Baligidad, A.C. Maharudresh, N. Dayanand, “Analysis of composite pressure vessel and composite overwrapped pressure vessel by analytical and finite elemental approach”, materialstoday: Proceedings, Vol.50, Part 5, pp.1726-1731 (2022).https://doi.org/10.1016/j.matpr.2021.09.174
22. Z. Hu, M. Chen, and B. Pan, “Simulation and burst validation of 70 MPa type IV hydrogen storage vessel with dome reinforcement”, Int J Hydrogen Energy, Vol. 46, No. 46, pp. 23779–23794 (2021). doi: 10.1016/j.ijhydene.2021.04.186.
23. E. Moskvichev, “Numerical modeling of stress-strain behavior of composite overwrapped pressure vessel”, Procedia Structural Integrity, Vol.2, pp. 2512–2518 (216). doi: 10.1016/j.prostr.2016.06.314.
24. H. Wang, S. Fu, Y. Chen, and L. Hua, “Thickness-prediction method involving tow redistribution for the dome of composite hydrogen storage vessels”, Polymers (Basel), Vol. 14, No. 5:905 (2022).doi: 10.3390/polym14050902.
25. A.P. Beena, M.K. Sundaresan and B. Nageswara Rao, "Destructive tests of 15CDV6 steel rocket motor cases and their application to lightweight design", International Journal of Pressure Vessels & Piping, Vol.62, pp.313-320 (1995).
26. K. Jayakumar, D. Yadav and B. Nageswara Rao, “A multi-layer cylindrical shell under electro-thermo-mechanical loads”, Trends in Applied Sciences Research, Vol.1, No.4, pp.386-404 (2006).
27. Jayakumar Krishnankutty, “Piezo-laminated beams, plates and shell with random actuation electric potential difference and material properties”, Ph. D thesis, Department of Aerospace Engineering, Indian Institute of Technology, Kanpur, India (December 2007)
28. P. Xu, J. Y. Zheng, and P. F. Liu, “Finite element analysis of burst pressure of composite hydrogen storage vessels”, Mater Des, Vol. 30, No. 7, pp. 2295–2301 (2009).doi: 10.1016/j.matdes.2009.03.006.
29. P.F. Liu and J.Y. Zheng, “Progressive failure analysis of carbon fiber/epoxy composite laminates using continuum damage mechanics”, Materials Science and Engineering A, Vol. 485, No. 1–2, pp. 711–717 (2008). doi: 10.1016/j.msea.2008.02.023.
30. Madhujit Mukhopadhyay, “Mechanics of Composite Materials and Structures”, Universities Press (India) Private Limited, Hyderabad, India (2022).

